Supporting Information

Coupled nanocomposite $Co_{5.47}N$-Co_3Fe_7 inlaid in tremella-like carbon framework as highly efficient multifunctional electrocatalyst for oxygen transformation and overall water splitting

Fantao Kong, Chaoqi Zhang, Yu Qiao, Ruijing Li, Aiguo Kong* and Yongkui Shan*

School of Chemistry and Molecular Engineering, East China Normal University, 500 Dong chuan Road, Shanghai 200241, P. R. China.

Corresponding Author: agkong@chem.ecnu.edu.cn, ykshan@chem.ecnu.edu.cn

CONTENTS

alkiline (A, B) and acidic (C, D) solutions.

Fig. S10. TEM images of $Co_{5.47}N@Co_3Fe_7$/N-C-900 before (A) and after the stability test in acidic (B) and alkaline (C) electrolytes.

Fig. S11. XRD pattern of the $Co_{5.47}N@Co_3Fe_7$/N-C-900 catalyst before and after ORR tests.

Fig. S12. The photograph of a light-emitting diode (LED, 3 V).

Video S1. $Co_{5.47}N@Co_3Fe_7$/N-C-900/NF||$Co_{5.47}N@Co_3Fe_7$/N-C-900/NF water electrolyzer at high current density. (AVI)

Table S1. The surface chemical compositions and relative content of different nitrogen species on N-C-aerogel and $Co_{5.47}N@Co_3Fe_7$/N-C-900 from the XPS spectra.

Table S2. The surface composition of different catalysts and the relative content of Co-N and Fe-N moieties on Co/N-C-900, Fe/N-C-900 and $Co_{5.47}N@Co_3Fe_7$/N-C-900 estimated from the XPS analysis.

Table S3. Comparison of ORR catalytic activity of $Co_{5.47}N@Co_3Fe_7$/N-C-900 in alkiline solution with the recently reported non-precious electrocatalysts in the literature.

Table S4. Comparison of ORR catalytic activity of $Co_{5.47}N@Co_3Fe_7$/N-C-900 in acidic solution with the recently reported non-precious electrocatalysts in the literature.

Table S5. Comparison of OER catalytic activity of $Co_{5.47}N@Co_3Fe_7$/N-C-900 in alkiline solution with the recently reported non-precious electrocatalysts in the literature.

Table S6. Comparison of electrocatalytic activities of $Co_{5.47}N@Co_3Fe_7$/N-C-900 with the recently reported catalysts for ORR and OER.

Table S7. Comparison of HER catalytic activity of $Co_{5.47}N@Co_3Fe_7$/N-C-900 in acidic or alkiline solution with the recently reported non-precious electrocatalysts in the literature.

Experimental section

Chemicals. All chemicals were purchased from Sinopharm Group Chemical Reagent Co., Ltd. and used without further purifcation.

Synthetic procedures

Synthesis of graphene oxides (GO). Graphene oxides was prepared from natural graphite (Alfa Aesar) by using a modified Hummers method.[S1] In a typical synthesis process, 5 g of graphite flakes were added into a 250 mL round-bottomed flask, which containing a solution of concentrated 98% H_2SO_4 (100 mL), P_2O_5 (2.5 g) and $K_2S_2O_8$ (2.5 g). Then the mixture was heated to 80 °C and stirred for 6 h to complete the pre-oxidation of graphite. After cooling in air, the preoxidized graphite was filtered, washed with deionized water to remove the residual acid and then dried in vacuum overnight at room temperature. 5 g of the preoxidized graphite and 115 mL of 98% H_2SO_4 were blended in a beaker in an ice-water bath. 15 g of $KMnO_4$ was added gradually to the above solution under vigorous stirring conditions below 10 °C, and after that, continue to stir for 2 h at 35 °C to complete the oxidation of graphite. 230 mL of deionized water was slowly added into the reaction mixture under vigorous stirring at approximately 100 °C. After the mixture was cooled to room temperature, and additional water (700 mL) and 30% H_2O_2 (12.5 mL) were added into it to reduce the residual permanganate and manganese dioxide. The color of the mixture changed from dark-brown to bright yellow suspension. Finally, the graphene oxides (GO) were obtained by washing with diluted HCl (3%) solution three times and dialysis (dialysis membrane retained molecular weight: 8000-14000 Da) for a week to remove the residual salts and acids.

Purification and oxidation of CNTs. 500 mg of the commercially available multi-walled carbon nanotubes (CNT, 10-30 nm in diameter, 5-15 μm in length, purity 95 wt %) were calcined in a muffle furnace at 500 °C for 2 h in air to burn some of the impurities in the carbon nanotubes. The calcined

carbon nanotubes were treated with concentrated hydrochloric acid under the sonicating conditions for 6 h to remove the residual of metal impurities. The purified CNTs were obtained by filtering, washing with deionized water to remove the residual acid and drying in vacuum at 60 °C. In order to prepare the carbon nanotube oxide, 300 mg of purified CNTs were added in a mixture of H_2SO_4/HNO_3 (3:1, v/v) and held for 8 h at 80 °C. The nanotube oxides were harvested by washing with deionized water until the pH of filtrate was close to neutral and dispersed into deionized water to form a uniform suspension. The concentration of the obtained oxidized carbon nanotubes (o-CNTs) was 1 mg/mL.

Synthesis of nitrogen-doped graphene/carbon nanotube aerogels (N-C-aerogel). In a typical synthesis process, 25 mL of GO dispersion (2 mg/mL) was mixed with 40 mL of o-CNT solution (1 mg/mL) and sonicated for 30 min to form the suspension. 24 g of urea was added to the mixed suspension and continued ultrasound treatment for 3 h then which was transferred to a poly(tetrafluoroethylene) (Teflon)-lined autoclave (100 mL) and heated at 180 °C for 12 h. After cooling to room temperature, the resulting black suspension was filtered through a 0.22-mm microporous membrane. The solid on the filter was freeze-dried overnight to obtain N-C-aerogel.

Assembly of the nitrogen-doped carbon embeding $Co_{5.47}N$ and Co_3Fe_7 coupled nanoparticles ($Co_{5.47}N@Co_3Fe_7$/N-Cs). Briefly, 0.4 g (1.48×10^{-3} mol) of iron(III) chloride hexahydrate ($FeCl_3\bullet6H_2O$) and 0.4 g (1.68×10^{-3} mol) of cobalt(II) chloride hexahydrate ($CoCl_2\bullet6H_2O$) were dissolved in ethanol of 20 mL by continuous ultrasound to form a dark green solution, and then the prepared N-C-aerogels were dispersed into the ethanol solution by ultrasound. The solvent was slowly evaporated under constantly stirring at room temperature to obtain solid residues, which was heated to 900 °C in the tube furnace at a heating rate of 2℃ min^{-1} and held for 4 hours with a flow of high-purity N_2 at same temperature. The resultant product was named nitrogen-doped carbon embeding

$Co_{5.47}N$ and Co_3Fe_7 coupled nanoparticles ($Co_{5.47}N@Co_3Fe_7$/N-C-900). For comparison, N-doped carbon (N-C-900), Fe-based N-doped carbon (Fe/N-C-900), Co-based N-doped carbon (Co/N-C-900) and $Co_{5.47}N@Co_3Fe_7$/N-C-X (X: heat treatment temperature) materials were also obtained by the similar preparation procedure except the heat treatment temperature and the reactants.

Characterization. Wide-angle powder X-ray diffraction (XRD) patterns were performed on a D8 Advance X-ray diffractometer (Bruker AXS, Germany) with Cu Kα radiation in the range from 10° to 80°. The surface morphology and composition of samples were characterized using a scanning electron microscope (Hitachi ST-4800 SEM). The microstructure of as-prepared samples were examined by using the transmission electron microscopy (TEM), elemental mapping and high-resolution TEM (HR-TEM) on a JEM-2010 instrument at an accelerating voltage of 200 kV. X-ray photoelectron spectroscopy (XPS) was performed using Axis Ultra DLD with Al Kα radiation (15 kV, 150 W) and the C 1s peak at 284.6 eV as an internal standard. N_2 adsorption-desorption isotherm measurements were carried on a Micromeritics ASAP 2020 analyzer at 77 K, the specific surface area and pore size distribution were obtained by the Brunauer-Emmett-Teller (BET) and Barrett-Joyner-Halenda (BJH) methods, respectively. Raman spectra were performed by using a GX-PT-1500 (150) instrument with a 532 nm excitation laser (1mW).

Electrode preparation and electrochemical measurement. The electrochemical measurements were carried out by cyclic voltammetry (CV) and rotating disk electrode (RDE) techniques operated on a standard three-electrode system connected to a CHI-760C workstatin and coupled with a rotating rink-disk electrode system (PINE, USA). A glassy carbon rotating disk electrode (5.6 mm in diameter, Pine) loading with various catalysts served as the working electrode, a Pt wire or graphite rod as a counter electrode, an Ag/AgCl electrode (KCl, 3 M) as the reference electrode. The catalyst ink were prepared by dispersing 10 mg of as-produced catalyst powder in a 1.28 mL ethanol solution

containing 30 μL Nafion (5 wt %) to form a homogeneous suspension in an ultrasonic bath. Then, the catalyst ink was pipetted onto a polished glassy carbon electrode (GC) and dried under ambient conditions before use. Before measurement, the electrolytes were saturated by bubbling N_2 or O_2 for 30 min. All potentials were calibrated to a reversible hydrogen electrode (RHE) (Fig. S1).

The ORR measurements were conducted in O_2-saturated 0.1 M KOH or 0.1 M $HClO_4$ solution at a scan rate of 5 mV s^{-1}. The polarization curves of ORR were corrected by subtracting the background double-layer current from the measured current in argon-saturated electrolytes. The catalysts loaded on the working electrode were approximately 0.6 mg cm^{-2} in alkaline electrolyte and 0.8 mg cm^{-2} in acidic electrolyte. The loading of Pt/C (JM) was 0.1 mg cm^{-2} in both electrolytes for comparison. The onset potential was defined as the electrode potential when ORR current density is 3 μA cm^{-2} in rotating disk electrode (RDE) polarization curves, according to the reported method in the literature.[S2,S3] Electrochemical impedance spectroscopy (EIS) was measured under the potential holding of -0.182 V vs. Ag/AgCl in O_2-saturated 0.1 M KOH solution in the frequency range of 1000 kHz to 0.01 Hz with an amplitude of 10 mV. Chronopotentiometry tests were performed to evaluate the stability and methanol resistance of the catalysts.

The numbers (n) of charge transferred per oxygen molecule toward ORR process were calculated by Koutecky-Levich (K-L) equations:

$$\frac{1}{J} = \frac{1}{J_k} + \frac{1}{J_L} = \frac{1}{J_k} + \frac{1}{B\omega^{1/2}} \quad (1)$$

$$B = 0.62nFC_0 D_0^{\frac{2}{3}} v^{-\frac{1}{6}} \quad (2)$$

$$J_k = nFkC_0 \quad (3)$$

where n is the overall number of electrons transferred in the ORR process, J is the measured current density, J_k is the kinetic current density, F is the Faradaic constant (F = 96485 C mol L^{-1}), C_0 is the

bulk concentration of O_2 in the electrolyte, D_0 is the diffusion coefficient of O_2, v is the kinematic viscosity of the electrolyte, and k is the electron transfer rate constant, and ω is the rotating speed of the electrode in the form of revolutions per minute (rpm). According to Equation (1), the ORR kinetic current could be calculated based on Equation (4).

$$J_k = \frac{J \times J_L}{J_L - J} \qquad (4)$$

Electrochemically active surface areas (EASAs) can be evaluated by the electrochemical double-layer capacitance (C_{dl}). Cyclic voltammetry (CV) cycles at different scan rates of 5-30 mV s^{-1} were conducted to measure the C_{dl} at non-faradaic overpotentials. A linear trend can be observed by plotting the difference value (ΔJ) against the CV scan rate between the anodic and cathodic sweeps at a specific potential (1.03-1.13 V *vs.* RHE). The EASA can be calculated as:

$$EASA = C_{dl}/C_S \qquad (5)$$

Cs is the specific capacitance value for a flat standard with 1 cm^{-2} of real surface area. The general value for *Cs* is 40 μF/cm^2.[S4]

For OER and HER, the measurements were performed in O_2-saturated 1.0 M KOH and N_2-saturated 0.5 M H_2SO_4 solutions respectively, where graphite rod was employed as the counter electrode for HER test. The final loading for all catalysts on GC electrode was 0.6 mg cm^{-2} in the OER and HER. The benchmark IrO_2 and Pt/C catalysts with the same mass loading as working electrode were utilized for investigation and comparison. The RDE tests were scanned at a scan rate of 5 mV s^{-1} with a rotation speed of 1600 rpm. All LSV curve potentials of OER and HER were iR-corrected by electrochemical impedance spectroscopy.

For ORR, OER and HER, the kinetic performance of as-prepared catalysts can be evaluated by the Tafel slope (b), which was obtained by fitting the linear part of the Tafel plots according to the Tafel equation ($\eta = a + b\log(j)$).

Zinc-air batteries assembly. A homemade Zn-air battery in a two-electrode system was assembled by loading the $Co_{5.47}N@Co_3Fe_7$/N-C catalyst (with a loading of 3 mg cm^{-2}) on a porous carbon cloth substrate as the air cathode. A polished Zn plate was utilized as the anode, and 6 M KOH with 0.2 M $Zn(Ac)_2$ mixed solution was applied as the electrolyte. The discharge polarization and power density plots were recorded using a galvanodynamic method. Charge/discharge cycling tests were performed on the LAND CT2001 instrument by 5 min charge step followed by 5 min discharge step with the same current density of 20 mA cm^{-2} for 24 h.

Water spilliting system test. Overall water spilliting was performed by a two-electrode configuration assembled by using $Co_{5.47}N@Co_3Fe_7$/N-C-900 as both the anode and cathode material and tested in 1 M KOH solution. The catalyst ink was prepared according to the steps above. The prepared suspensions were then coated on a Ni foam (NF) substrate of ~1.0 cm^2 in area and dried under ambient conditions. The mass loading of catalysts was about 4.5 mg cm^{-2}. Before use, the nickel foam substrates were ultrasonically cleaned with 3 M HCl (38%) solution, ethanol and distilled water for a few minutes.

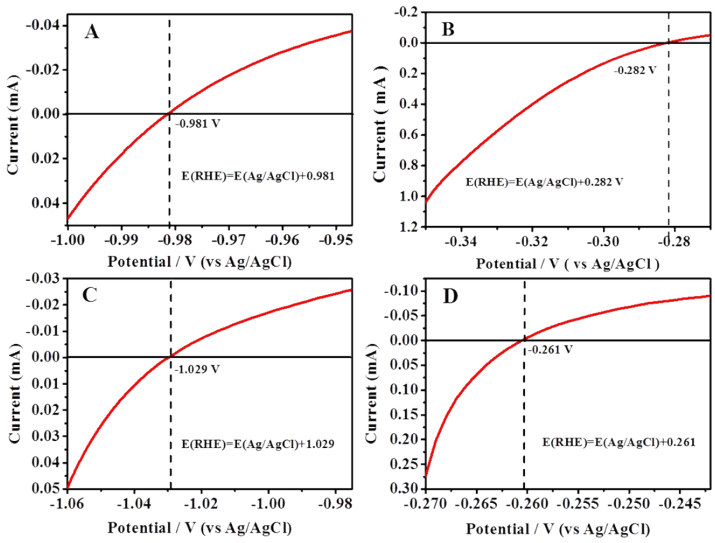

Fig. S1. Calibration to reversible hydrogen electrode (RHE) in 0.1 M KOH (A), 0.1 M $HClO_4$ (B), 1 M KOH (C) and 0.5 M H_2SO_4 (D) electrolytes.

All the reported potentials in our paper were calibrated to the RHE potentials according to the reported method.[S3] The calibration was performed in a standard three-electrode system with platinum wires as the working and counter electrodes, and the Ag/AgCl electrode as the reference electrode. Linear scanning voltammetry (LSV) was then run at a scan rate of 5 mV s^{-1}, and the potential at which the current crossed zero is taken to be the thermodynamic potential for the hydrogen electrode reactions (Fig. S1).

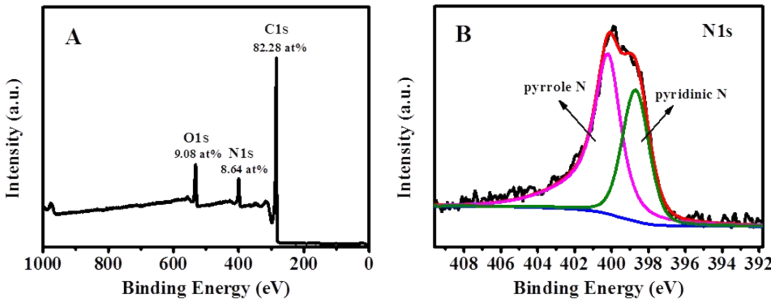

Fig. S2. The survey (A) and high-resolution N1s (B) XPS spectra of the N-C-aerogel.

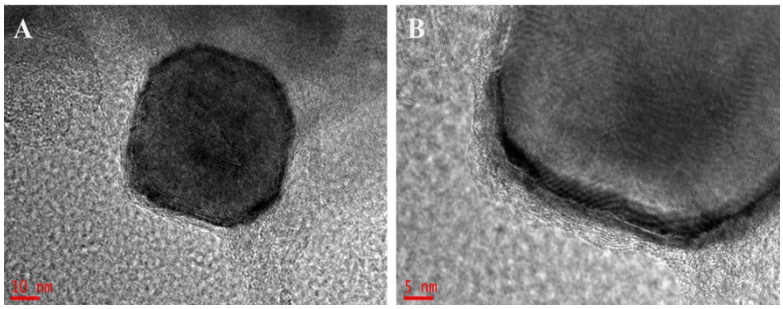

Fig. S3. TEM images of the prepared $Co_{5.47}N@Co_3Fe_7$/N-C-900 with distinct border.

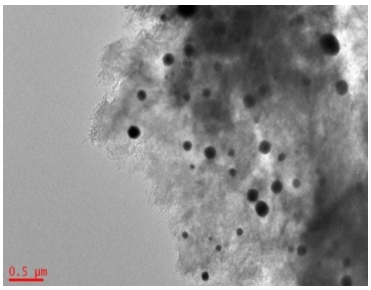

Fig. S4. TEM image of $Co_{5.47}N@Co_3Fe_7$/N-C-1000.

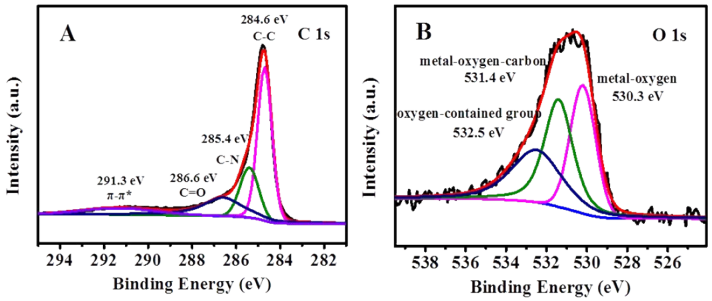

Fig. S5. (A) C_{1s} and (B) O_{1s} high-resolution XPS spectra of the $Co_{5.47}N@Co_3Fe_7$/N-C-900 along with the corresponding fitting curves.

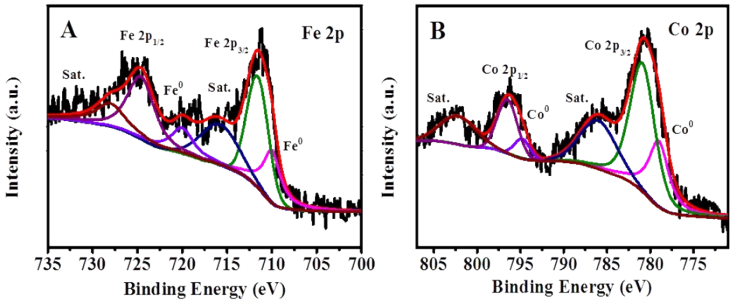

Fig. S6. (A) Fe_{2p} XPS spectra of the Fe/N-C-900 and (B) Co_{2p} XPS spectra of the Co/N-C-900.

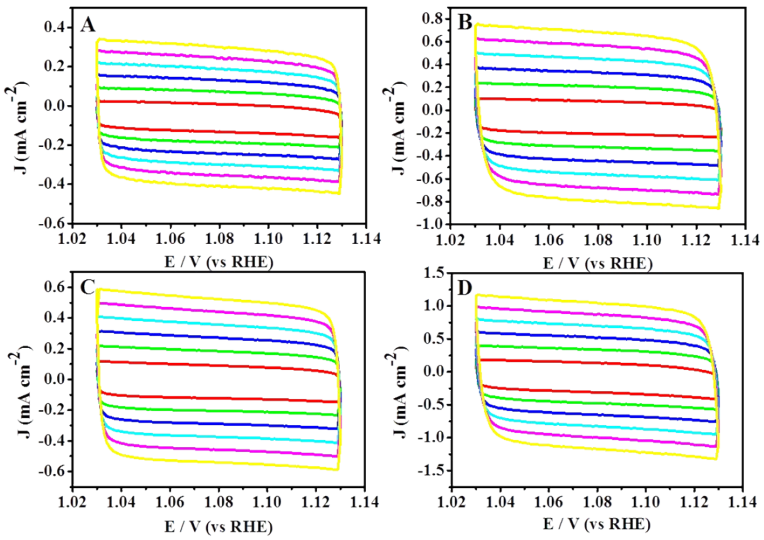

Fig. S7. CV curves of N-C (A), Fe/N-C (B), Co/N-C (C), and $Co_{5.47}N@Co_3Fe_7$/N-C-900 (D) conducted in 0.1 M KOH at scan rates of 5 mV/s, 10 mV/s, 15 mV/s, 20 mV/s, 25 mV/s and 30 mV/s.

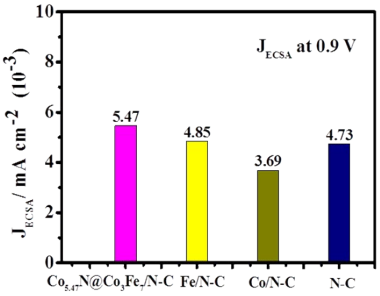

Fig. S8. Comparison of the ECSA normalized current density of N-C-900, Co/N-C-900, Fe/N-C-900 and $Co_{5.47}N@Co_3Fe_7$/N-C-900 measured at 0.9 V vs. RHE in 0.1 M KOH electrolyte.

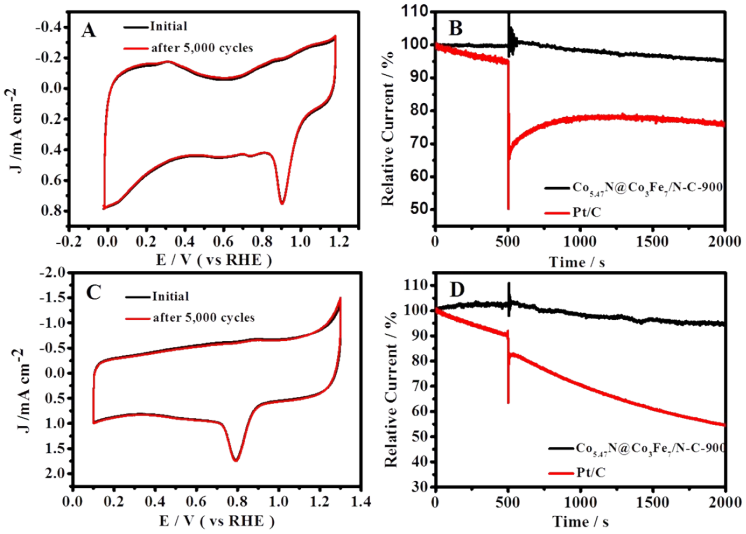

Fig. S9. CVs run for 5000 cycles of $Co_{5.47}N@Co_3Fe_7$/N-C-900 recorded in O_2-saturated 0.1 M KOH (A) and 0.1 M $HClO_4$ (C) solution. Current-time (i-t) chronoamperometric response of $Co_{5.47}N@Co_3Fe_7$/N-C-900 and Pt/C-JM with the addition of methanol (3 wt %) in O_2-saturated 0.1 M KOH (B) and 0.1 M $HClO_4$ (D) solution.

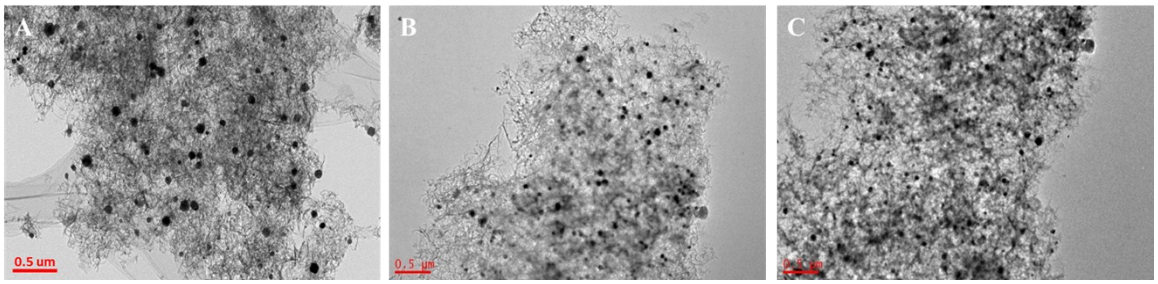

Fig. S10. TEM images of $Co_{5.47}N@Co_3Fe_7$/N-C-900 before (A) and after the stability test in acidic (B) and alkaline (C) electrolytes.

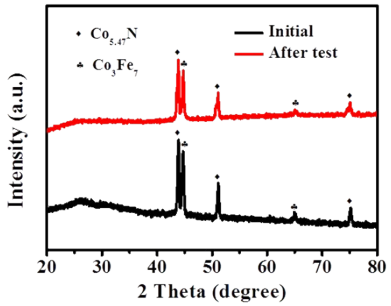

Fig. S11. XRD pattern of the $Co_{5.47}N@Co_3Fe_7$/N-C-900 catalyst before and after ORR tests.

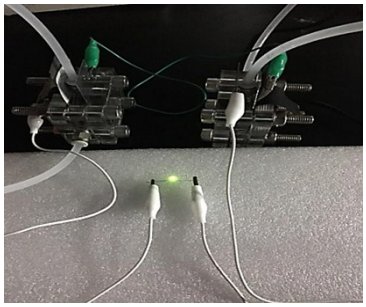

Fig. S12. Photograph of a light-emitting diode (LED, 3 V) powered by two batteries connected in series.

Table S1. The surface chemical compositions and relative content of different nitrogen species on N-C-aerogel and $Co_{5.47}N@Co_3Fe_7$/N-C-900 from the XPS spectra.

Samples	Element composition (at. %)					Relative content (%)				
	C	N	O	Fe	Co	Py-N	M-N_x	Pyr-N	G-N	NO_x
N-C-aerogel	78.46	8.64	12.9	—	—	36.0	—	64.0	—	—
$Co_{5.47}N@Co_3Fe_7$/N-C	88.91	1.64	5.68	1.87	1.90	14.7	49.5	—	24.8	11.0

Table S2. The surface composition of different catalysts and the relative content of Co-N and Fe-N moieties on Co/N-C-900, Fe/N-C-900 and $Co_{5.47}N@Co_3Fe_7$/N-C-900 estimated from the XPS analysis.

Samples	Element composition （at. %）				Relative content（%）		
	C	N	O	Co	Fe	Co-N	Fe-N
Co/N-C-900	90.54	2.85	4.30	2.31	—	49.6	—
Fe/N-C-900	91.47	2.55	3.82	—	2.16	—	43.5
$Co_{5.47}N@Co_3Fe_7$/N-C-900	88.91	1.64	5.68	1.90	1.87	52.0	59.6

Table S3. Comparison of ORR catalytic activity of $Co_{5.47}N@Co_3Fe_7$/N-C-900 in alkaline electrolyte with the recently reported non-precious electrocatalysts in the literature.

Catalysts	Loading mg/cm^2	Onset potential (V vs. RHE)	Half-wave potential (V vs. RHE)	Electrolyte	Ref
Co_4N/CNW/CC	—	—	0.80	1.0 M KOH	S6
FeCo/C-800	0.20	1.00	0.85	0.1 M KOH	S7
FeCo-OMPC	0.30	1.00	0.86	0.1 M KOH	S8
N-GCNT/FeCo-3	0.20	1.00	0.92	0.1 M KOH	S9
Fe-ISAs/CN	0.41	0.986	0.90	0.1 M KOH	S10
$Fe_{0.3}Co_{0.7}$/NC	0.25	0.98	0.88	0.1 M KOH	S11
FeCo-Co_4N/N-C	0.30	—	0.76	0.1 M KOH	S12
FeCo /NPC	0.485	—	0.78	0.1 M KOH	S13
FeCo @NC-800	0.42	0.975	0.88	0.1 M KOH	S14
CoFe/N-GCT	0.60	0.91	0.79	0.1 M KOH	S15
$Co_{1.08}Fe_{3.34}$	0.20	1.03	0.92	0.1 M KOH	S16
FeCo@N,S-CNT-800	0.20	0.954	0.838	0.1 M KOH	S17
FeCo@MNC	0.36	—	0.86	0.1 M KOH	S18
meso/micro-FeCo-N_x	0.10	0.954	0.886	0.1 M KOH	S19
FeCo@C MS	0.255	1.04	0.85	0.1 M KOH	S20
DG@FeCo	0.16	0.95	0.816	0.1 M KOH	S21
FeCNF-NP	0.60	0.98	0.88	0.1 M KOH	S22
Fe-N_4 SAs/NPC	0.51	0.972	0.885	0.1 M KOH	S23
Pt/C-JM	0.10	1.04	0.85	0.1 M KOH	This work
$Co_{5.47}N@Co_3Fe_7$/N-C	0.60	1.10	0.94	0.1 M KOH	This work

Table S4. Comparison of ORR catalytic activity of $Co_{5.47}N@Co_3Fe_7$/N-C-900 in acidic electrolytes with the recently reported non-precious electrocatalysts in the literature.

Catalysts	Loading mg/cm^2	Half-wave potential (V vs. RHE)	Electrolyte	Ref.
FeCo/C-800	0.60	0.75	0.1M $HClO_4$	S7
FeCo-OMPC	0.60	0.85	0.1M $HClO_4$	S8
$Co_{1.08}Fe_{3.34}$	0.32	0.78	0.1M $HClO_4$	S16
FeCo@C MS	0.255	0.60	0.5M H_2SO_4	S20
PANI-FeCo-C	0.60	0.80	0.5M H_2SO_4	S24
FeMo-C/N-3	0.10	0.67	0.5M H_2SO_4	S25
Fe/Co-CMP-800	0.60	0.78	0.5M H_2SO_4	S26
VB_{12}/silica colloid	0.60	0.79	0.5M H_2SO_4	S27
Fe_3C/NG-800	0.40	0.77	0.1M $HClO_4$	S28
CPANI-Fe-NaCl	0.60	0.73	0.1M $HClO_4$	S29
Fe-N-C-3HT-2AL	0.80	0.84	0.1M $HClO_4$	S30
PPy/FeTCPP/Co	0.30	0.72	0.1M $HClO_4$	S31
Co@SACo-N-C-10	0.60	0.78	0.1M $HClO_4$	S32
Pt-JM	0.10	0.80	0.1M $HClO_4$	This work
$Co_{5.47}N@Co_3Fe_7$/N-C	0.81	0.80	0.1M $HClO_4$	This work

Table S5. Comparison of OER catalytic activity of $Co_{5.47}N@Co_3Fe_7$/N-C-900 in alkaline electrolytes with the recently reported non-precious electrocatalysts in the literature.

Catalysts	Loading mg/cm^2	Overpotential at 10 mA cm^{-2} (mV vs. RHE)	Tafel slope (mV dec^{-1})	Electrolyte	Ref.
Co_4N/CNW/CC	—	310	81	1.0 M KOH	S6
N-GCNT/FeCo-3	0.2	500	99.5	0.1 M KOH	S9
FeCo/NPC	0.485	440	85	0.1 M KOH	S13
CoFe/N-GCT	0.6	440	106	0.1 M KOH	S15
FeCo@MNC	0.36	240	60	1.0 M KOH	S17
meso/micro-FeCo-Nx	0.10	370	57	1.0 M KOH	S19
FeCo@C MS	0.255	440	—	0.1 M KOH	S20
Fe-N_4 SAs/NPC	0.51	430	95	1.0 M KOH	S23
Co3Fe7Ni-2	0.32	325	60	1.0 M KOH	S33
$Co_{0.75}Fe_{0.25}$-NC	0.212	303	30	1.0 M KOH	S34
FeCo@NG/NCNT	0.14	450	77	1.0 M KOH	S35
$Fe_{0.5}Co_{0.5}$@NC/NCNS	0.306	270	50	1.0 M KOH	S36
FeCoOOH/NF	—	211	33	1.0 M KOH	S37
Ni_2P/CoN–PCP	0.26	270	65	1.0 M KOH	S38
Fe_2N/S/N	0.4	360	57	1.0 M KOH	S39
$FeNi_3N$/NG	0.1	258	85	1.0 M KOH	S40
Fe/P/$C_{0.5}$-800	0.46	330	67	1.0 M KOH	S41
IrO_2	0.45	320	63	1.0 M KOH	This work
$Co_{5.47}N@Co_3Fe_7$/N-C	0.6	310	69	1.0 M KOH	This work

Table S6. Comparison of electrocatalytic activities of $Co_{5.47}N@Co_3Fe_7$/N-C-900 with the recently reported catalysts for ORR and OER.

Catalyst	$E_{1/2}$ (V vs. RHE)	$E_{j=10}$ (V vs. RHE)	ΔE(V)	Loading (mg cm^{-2})	Electrolytes	Ref.
Co_4N/CNW/CC	0.80	1.54	0.74	—	1 M KOH	S6
N-GCNT/FeCo-3	0.92	1.73	0.81	0.2	0.1 M KOH	S9
CoFe/N-GCT	0.79	1.67	0.88	0.6	0.1 M KOH	S15
Co/NC	0.83	1.69	0.86	0.21	0.1 M KOH	S42
Fe@N-C 700	0.83	1.71	0.88	0.31	0.1 M KOH	S43
CoFe@NCNTs	0.84	1.68	0.84	0.8	0.1 M KOH	S44
Co_3O_4/NBGHS	0.86	1.71	0.85	—	0.1 M KOH	S45
NCNF-1000	0.82	1.84	1.02	0.1	0.1 M KOH	S46
NCN-1000-5	0.82	1.61	0.81	0.2	0.1 M KOH	S47
$CoFe_2O_4$/bicarbon	0.70	1.65	0.95	0.503	0.1 M KOH	S48
$NiCo_2S_4$/N-CNT	0.8	1.60	0.8	0.248	0.1 M KOH	S49
IrO_2	0.27	1.67	1.4	0.45	0.1 M KOH	This work
Pt/C	0.84	1.97	1.13	0.1	0.1 M KOH	This work
$Co_{5.47}N@Co_3Fe_7$/N-C	0.94	1.72	0.78	0.6	0.1 M KOH	This work

Table S7. Comparison of HER catalytic activity of $Co_{5.47}N@Co_3Fe_7$/N-C-900 with the recently reported non-precious electrocatalysts in the literature.

Catalysts	Loading mg/cm^2	Overpotential at 10 mA cm^{-2} (mV vs. RHE)	Tafel slope (mV dec^{-1})	Electrolytes	Ref.
FeCo/NPC	0.6	340	125	1.0 M KOH	S14
FeCo@C MS	0.255	220	65	0.5 M H_2SO_4	S21
FeCo	0.32	211	77	1.0 M KOH	S33
$Co_{0.75}Fe_{0.25}$-NC	0.212	202	68	1.0 M KOH	S34
FeCo@NG/NCNT	0.14	332	110	0.5 M H_2SO_4	S35
Ni_2P/CoN-PCP	0.26	94	41	1.0 M KOH	S38
$FeNi_3N$/NG	0.1	186	83	1.0 M KOH	S39
Co_3O_4/NCMTs	1.0	210	—	1.0 M KOH	S40
Co@N-CNTF	0.28	220	—	1.0 M KOH	S41
FeCo@N-C	0.6	230	92	0.5 M H_2SO_4	S50
FeCo@N-C/KB	0.6	240	97	0.5 M H_2SO_4	S50
FeCo@NCNTs-NH	0.32	276	74	0.1 M H_2SO_4	S51
Co_2P/CoN-NCNT	0.2	98	57	0.5 M H_2SO_4	S52
$(Fe_{0.75}Co_{0.25})_5C_2$	0.71	174	—	0.1 M KOH	S53
$(Ni,Co)S_2$	—	180	68	0.1 M KOH	S54
Co/CoP–HNC	0.19	181	104	1.0 M KOH	S55
Pt/C	0.6	30	45	0.5 M H_2SO_4	This work
$Co_{5.47}N@Co_3Fe7$/N-C	0.6	115	68	0.5 M H_2SO_4	This work
$Co_{5.47}N@Co_3Fe_7$/N-C	0.6	181	112	1.0 M KOH	This work

References

[S1] W. S. Hummers Jr and R. E. Offeman, *J. Am. Chem. Soc.*, 1958, **80**, 1339-1339.

[S2] M. Chokai, M. Taniguchi, S. Moriya, K. Matsubayashi, T. Shinoda, Y. Nabae, S. Kuroki, T. Hayakawa, M.-a. Kakimoto and J.-i. Ozaki, *J. Power Sour.*, 2010, **195**, 5947-5951.

[S3] A. Kong, X. Zhu, Z. Han, Y. Yu, Y. Zhang, B. Dong and Y. Shan, *ACS Catal.*, 2014, **4**, 1793-1800.

[S4] P. Li, H. Jang, B. Yuan, Z. Wu, X. Liu and J. Cho, *Inorg. Chem. Front.*, 2019, **6**, 417-422.

[S5] Y. Liang, Y. Li, H. Wang, J. Zhou, J. Wang, T. Regier and H. Dai, *Nat. Mater.*, 2011, **10**, 780.

[S6] F. Meng, H. Zhong, D. Bao, J. Yan and X. Zhang, *J. Am. Chem. Soc.*, 2016, **138**, 10226-10231.

[S7] Q. Lin, X. Bu, A. Kong, C. Mao, F. Bu and P. Feng, *Adv. Mater.*, 2015, **27**, 3431-3436.

[S8] J. Y. Cheon, T. Kim, Y. Choi, H. Y. Jeong, M. G. Kim, Y. J. Sa, J. Kim, Z. Lee, T.-H. Yang and K. Kwon, *Sci. Rep.*, 2013, **3**, 2715.

[S9] C. Y. Su, H. Cheng, W. Li, Z. Q. Liu, N. Li, Z. Hou, F. Q. Bai, H. X. Zhang and T. Y. Ma, *Adv. Energy Mater.*, 2017, **7**, 1602420.

[S10] Y. Chen, S. Ji, Y. Wang, J. Dong, W. Chen, Z. Li, R. Shen, L. Zheng, Z. Zhuang and D. Wang, *Angew. Chem. Int. Ed.*, 2017, **56**, 6937-6941.

[S11] B. Y. Guan, Y. Lu, Y. Wang, M. Wu and X. W. Lou, *Adv. Funct. Mater.*, 2018, **28**, 1706738.

[S12] X. Zhu, T. Jin, C. Tian, C. Lu, X. Liu, M. Zeng, X. Zhuang, S. Yang, L. He and H. Liu, *Adv. Mater.*, 2017, **29**, 1704091.

[S13] H. X. Zhong, J. Wang, Q. Zhang, F. Meng, D. Bao, T. Liu, X. Y. Yang, Z. W. Chang, J. M. Yan and X. B. Zhang, *Adv. Sustainable Syst.*, 2017, **1**, 1700020.

[S14] J. Tong, W. Wang, Q. Li, F. Liu, W. Ma, W. Li, B. Su, Z. Lei and L. Bo, *Electrochim. Acta*, 2017, **248**, 388-396.

[S15] X. Liu, L. Wang, P. Yu, C. Tian, F. Sun, J. Ma, W. Li and H. Fu, *Angew. Chem. Int. Ed*, 2018, **130**, 16398-16402.

[S16] S. Sultan, J. N. Tiwari, J. H. Jang, A. M. Harzandi, F. Salehnia, S. J. Yoo and K. S. Kim, *Adv. Energy Mater.*, 2018, **8**, 1801002.

[S17] D. Zhao, L. Li, L. Xie, N. Zhou and S. Chen, *J. Alloys Compd.*, 2018, **741**, 368-376.

[S18] C. Li, M. Wu and R. Liu, *Appl. Catal. B: Environ.*, 2019, **244**, 150-158.

[S19] S. Li, C. Cheng, X. Zhao, J. Schmidt and A. Thomas, *Angew. Chem. Int. Ed.*, 2018, **57**, 1856-1862.

[S20] W. Zang, A. Sumboja, Y. Ma, H. Zhang, Y. Wu, S. Wu, H. Wu, Z. Liu, C. Guan and J. Wang, *ACS Catal.*, 2018, **8**, 8961-8969.

[S21] X. Yan, Y. Jia, L. Zhang, M. T. Soo and X. Yao, *Chem. Commun.*, 2017, **53**, 12140-12143.

[S22] M. Wang, C. Zhang, T. Meng, Z. Pu, H. Jin, D. He, J. Zhang and S. Mu, *J. Power Source*, 2019, **413**, 367-375.

[S23] Y. Pan, S. Liu, K. Sun, X. Chen, B. Wang, K. Wu, X. Cao, W. C. Cheong, R. Shen and A. Han, *Angew. Chem. Int. Ed.*, 2018, **57**, 8614-8618.

[S24] G. Wu, K. L. More, C. M. Johnston and P. Zelenay, *Science*, 2011, **332**, 443-447.

[S25] L. Lin, Z. K. Yang, Y.-F. Jiang and A.-W. Xu, *ACS Catal.*, 2016, **6**, 4449-4454.

[S26] J. Yang, H. Guo, S. Chen, Y. Li, C. Cai, P. Gao, L. Wang, Y. Zhang, R. Sun and X. Niu, *J. Mater. Chem. A*, 2018, **6**, 13859-13866.

[S27] H.-W. Liang, W. Wei, Z.-S. Wu, X. Feng and K. Müllen, *J. Am. Chem. Soc.*, 2013, **135**, 16002-16005.

[S28] M. Xiao, J. Zhu, L. Feng, C. Liu and W. Xing, *Adv. Mater.*, 2015, **27**, 2521-2527.

[S29] W. Ding, L. Li, K. Xiong, Y. Wang, W. Li, Y. Nie, S. Chen, X. Qi and Z. Wei, *J. Am. Chem.*

Soc., 2015, **137**, 5414-5420.

[S30] N. R. Sahraie, U. I. Kramm, J. Steinberg, Y. Zhang, A. Thomas, T. Reier, J.-P. Paraknowitsch and P. Strasser, *Nat. Commun.* 2015, **6**, 8618.

[S31] J. Yang, X. Wang, B. Li, L. Ma, L. Shi, Y. Xiong and H. Xu, *Adv. Funct. Mater.*, 2017, **27**, 1606497.

[S32] Q. Cheng, S. Han, K. Mao, C. Chen, L. Yang, Z. Zou, M. Gu, Z. Hu and H. Yang, *Nano Energy*, 2018, **52**, 485-493.

[S33] Y. Yang, Z. Lin, S. Gao, J. Su, Z. Lun, G. Xia, J. Chen, R. Zhang and Q. Chen, *ACS Catal.*, 2016, **7**, 469-479.

[S34] X. Feng, X. Bo and L. Guo, *J. Power Sources*, 2018, **389**, 249-259.

[S35] B. Du, Q.-T. Meng, J.-Q. Sha and J.-S. Li, *New J. Chem.*, 2018, **42**, 3409-3414.

[S36] M. Li, T. Liu, X. Bo, M. Zhou and L. Guo, *J. Mater. Chem. A*, 2017, **5**, 5413-5425.

[S37] T. T. H. Nguyen, J. Lee, J. Bae and B. Lim, *Chem. -Eur. J.*, 2018, **24**, 4724-4728.

[S38] T. Sun, S. Zhang, L. Xu, D. Wang and Y. Li, *Chem Commun*, 2018, **54**, 12101-12104.

[S39] A. Mahmood, H. Tabassum, R. Zhao, W. Guo, W. Aftab, Z. Liang, Z. Sun and R. Zou, *Small*, 2018, **14**, 1803500.

[S40] L. Liu, F. Yan, K. Li, C. Zhu, Y. Xie, X. Zhang and Y. Chen, *J. Mater. Chem. A*, 2019, **7**, 1083-1091.

[S41] M. Li, T. Liu, X. Bo, M. Zhou, L. Guo and S. Guo, *Nano Energy*, 2017, **33**, 221-228.

[S42] A. Aijaz, J. Masa, C. Rösler, W. Xia, P. Weide, A. J. Botz, R. A. Fischer, W. Schuhmann and M. Muhler, *Angew. Chem. Int. Ed.*, 2016, **55**, 4087-4091.

[S43] J. Wang, H. Wu, D. Gao, S. Miao, G. Wang and X. Bao, *Nano Energy*, 2015, **13**, 387-396.

[S44] P. Cai, Y. Hong, S. Ci and Z. Wen, *Nanoscale*, 2016, **8**, 20048-20055.

[S45] Z. Jiang, Z.-J. Jiang, T. Maiyalagan and A. Manthiram, *J. Mater. Chem. A*, 2016, **4**, 5877-5889.

[S46] Q. Liu, Y. Wang, L. Dai and J. Yao, *Adv. Mater.*, 2016, **28**, 3000-3006.

[S47] H. Jiang, J. Gu, X. Zheng, M. Liu, X. Qiu, L. Wang, W. Li, Z. Chen, X. Ji and J. Li, *Energy Environ. Sci.*, 2019, **12**, 322-333.

[S48] S. Liu, W. Bian, Z. Yang, J. Tian, C. Jin, M. Shen, Z. Zhou and R. Yang, *J. Mater. Chem. A*, 2014, **2**, 18012-18017.

[S49] X. Han, X. Wu, C. Zhong, Y. Deng, N. Zhao and W. Hu, *Nano Energy*, 2017, **31**, 541-550.

[S50] S. H. Noh, M. H. Seo, J. Kang, T. Okajima, B. Han and T. Ohsaka, *NPG Asia Mater.*, 2016, **8**, e312.

[S51] J. Deng, P. Ren, D. Deng, L. Yu, F. Yang and X. Bao, *Energy Environ. Sci.*, 2014, **7**, 1919-1923.

[S52] Y. Guo, P. Yuan, J. Zhang, H. Xia, F. Cheng, M. Zhou, J. Li, Y. Qiao, S. Mu and Q. Xu, *Adv. Funct. Mater.*, 2018, **28**, 1805641.

[S53] S. Li, P. Ren, C. Yang, X. Liu, Z. Yin, W. Li, H. Yang, J. Li, X. Wang and Y. Wang, *Sci. Bull.*, 2018, **63**, 1358-1363.

[S54] J. Zhang, X. Bai, T. Wang, W. Xiao, P. Xi, J. Wang, D. Gao and J. Wang, *Nano-Micro Lett.*, 2019, **11**, 2.

[S55] Y. Hao, Y. Xu, W. Liu and X. Sun, *Mater. Horiz.*, 2018, **5**, 108-115.